JOURNAL OF GUIDANCE, CONTROL, AND DYNAMICS
Vol. 24, No. 2, March–April 2001

Robust Synergetic Design of Structural Dynamic Engine Out Controllers in Parameter Space

Michael Kordt* and Jürgen Ackermann†
DLR, German Aerospace Research Center, Oberpfaffenhofen, D-82234 Wessling, Germany

Engine out is a design criterion for a large transport aircraft from the viewpoint of flight safety, handling qualities, and structural dynamics. A structural dynamic engine out controller covers these aspects, especially the reduction of the loads level at the vertical tail. It is designed by a new robust synergetic design method, using Ackermann's parameter space method (Ackermann, J., *Robust Control*, Springer-Verlag, Berlin, 1993, Chap. 11, pp. 307–353). It allows the combination of different controller structures, each of which satisfies specific requirements. This combination of controllers robustly satisfies all of the multidisciplinary requirements. Here, three controllers are combined: a standard lateral controller and a proportional–integral controller for safety and handling qualities and a structural dynamic controller, which robustly decouples the shear force at the vertical tail from the yaw rate. This unilateral decoupling controller achieves an early efficient yawing moment compensation before the pilot. The controller consists of a feedback of the yaw rate to the rudder. Thereby, critical flight and load conditions due to a delayed overreaction of the pilot are prevented. The three controllers are characterized by eigenvalue regions for the closed-loop system. These Γ regions offer compromises between the conflicts in design goals. Using the parameter space method, this approach yields a set of robust controllers. A controller is selected and simulated on a nonlinear model.

I. Introduction

THE present day standard of safety clearly is to be maintained for the next generation of large transport aircraft. Availability of fly-by-wire offers additional potential to increase the flight safety and the handling quality (HQ) beyond the present level. This potential may become mandatory for a large capacity aircraft. One issue of concern is the mastering of an engine failure or engine out (EO) event, which can be accomplished by an EO controller or a thrust asymmetry controller.[1] Although the EO event is rather rare in normal aircraft (AC) operation, it is a well-trained pilot procedure. It is an AC design criterion in many respects: for AC configuration; for HQ, safety, and comfort; and for structural integrity and loads. Therefore an EO controller has to 1) master the transients following an EO and thereby allow the pilot to interact smoothly; 2) avoid dangerous loads and flight conditions from delayed pilot interference or an overreaction of the pilot, as defined by FAR/JAR 25.367,[2] (Note that there is no significant difference between JAR 25.367 and FAR 25.367.) or even from an adverse pilot reaction; and 3) avoid, in particular, excessive stress on the structure of an aircraft with an effect on the design loads level.[3] Mechanization of these general EO requirements must show robustness with respect to 1) parameter variations inside the flight envelope,[3] 2) variations in AC design mass conditions,[3] and 3) early design uncertainties, production tolerances, and design modifications. Most previous work in EO control has focused on simultaneously improving the HQ[1,4,5] and robustness.[6–8] The loads aspect, that is, the structural dynamic viewpoint, was not tackled. The purpose of this paper is to show that the loads aspect can be robustly integrated into the controller design.

Such a multidisciplinary controller design is here achieved by the following approach: Instead of trying to fulfill the cited multidisciplinary requirements by using one controller design methodology, several methodologies are adequately combined. Such synergetic controller design methodologies were analyzed in some recent papers on the design of flight control systems. In Ref. 9, eigenstructure assignment and linear quadratic regulator (LQR) design were adequately combined to fulfill HQ and aeroelastic requirements. In Refs. 7 and 8, both LQR design and pole placement were successfully combined with a design methodology based on a multidisciplinary optimization (multiobjective parameter synthesis) and applied to a robust autopilot design. Here, it will be shown that the parameter space method[10,11] is suitable for a robust synergetic combination of several linear time invariant controller structures: a standard lateral basis controller structure for stability augmentation, a proportional–integral–multiple input multiple output (PI–MIMO) controller, and a robust unilateral decoupling controller. Robust unilateral decoupling means that the lateral acceleration at a certain point of the aircraft is robustly decoupled from the yaw rate, but not vice versa.

The resulting controller is designed as a stability augmentation system (SAS), keeping the controller as simple and physically transparent as possible. The controller stabilizes the aircraft within 1 s after the detection. The aircraft is then in a flight condition with a nearly ideal sideslip angle and is near the corresponding trim point, that is, with a small bank angle and aileron deflections. Because of the slight perturbation, the pilot has no reason for any lateral overreaction. Considering the lateral SAS together with the EO controller design offers two possibilities of integrating the EO controller into the electronic flight control system (EFCS), that is, switching the controller on after a conventional detection of the engine failure or fully integrating the EO controller into the lateral basis controller. This choice will depend on the considered HQ requirements and is, therefore, beyond the scope of this paper.

The benefits in robustness and HQ from enlarging the EO controller to a command and stability augmentation system (CSAS) are exemplified by a standard command system for turn coordination: A robust multidisciplinary SAS is the best starting point for a robust multidisciplinary CSAS. Therefore, the way to achieve such a robust SAS by the robust synergetic design in parameter space is mostly emphasized.

The most critical EFCS mode in case of an EO from the structural dynamic viewpoint is the normal law. This is the standard CSAS taking advantage of all available sensors. Here, a pilot panic reaction might occur because the pilot is in the loop. Lower augmented EFCS modes such as direct or alternate law seem to be less critical because here the pilot is more engaged in the control process. When the

Received 22 April 1999; revision received 13 July 2000; accepted for publication 10 August 2000.

*Research Engineer, Institute of Robotics and Mechatronics; also Research Engineer, DaimlerChrysler Aerospace Airbus GmbH, Kreetslag 10, D-21129 Hamburg, Germany; michael.kordt@airbus.dasa.de and michael.kordt@dlr.de.

†Director, Institute of Robotics and Mechatronics.

autopilot is considered, there is a common agreement that, by using outer feedback loops, the change in flight condition as a result of an EO is more moderate than when using the normal law. Therefore, in the autopilot mode, there is no reason for an overreaction of the pilot. A recent example is the total energy/total heading control system.[12] Therefore, the present paper only tackles the normal law.

II. Modeling for Controller Design

An EO or engine failure can be modeled by a time-dependent disturbance in yawing moment (Fig. 1). As in standard lateral control system design, only the linear lateral rigid-body model is considered as a synthesis model. It is based on lateral derivatives including the α effect.[13] Nonlinear coupling terms between the longitudinal and the lateral motion, the nonlinear gravity, and the aerodynamic terms are assumed to be negligible. These and the following assumptions have to be verified via a high-precision model of the closed-loop system, covering these aspects exactly. The lateral model consists of one translational (sideslip angle β) and two rotational (yaw rate r and roll rate p) degrees of freedom, described by Newton and Euler equations.

Adding the bank angle ϕ and the heading angle ψ to the model yields the lateral state-space vector,[13] that is, $\boldsymbol{x} = [\phi,\ \psi,\ \beta,\ p,\ r]^T$. Because the nonlinear effect of the aileron–spoiler gearing is expected to be negligible, only rudder and aileron angles are considered as inputs $\boldsymbol{u} = [\delta_R,\ \delta_A]^T$. Moreover, the deflection rates and amplitudes are assumed to be always smaller than the rate and amplitude limitations. Finally, the EO yawing moment as disturbance input $z = [N_{z,D}]$ yields the standard linear state-space model as a multimodel[10] in the body axis,[13,14]

$$\Sigma: \dot{\boldsymbol{x}} = \boldsymbol{A}_{(i)}\boldsymbol{x} + \boldsymbol{B}_{(i)}\boldsymbol{u} + \boldsymbol{E}z, \qquad \boldsymbol{y} = \boldsymbol{x}, \qquad i = 1, \ldots, n_\Sigma \tag{1}$$

$$\boldsymbol{A}_{(i)} = \begin{bmatrix} 0 & 0 & 0 & 1 & 0 \\ 0 & 0 & 0 & 0 & 1 \\ g/V_{\mathrm{TAS}}(i) & 0 & Y_\beta(i) & Y_p(i) & Y_r(i) - 1 \\ 0 & 0 & L_\beta(i) & L_p(i) & L_r(i) \\ 0 & 0 & N_\beta(i) & N_p(i) & N_r(i) \end{bmatrix}$$

$$\boldsymbol{B}_{(i)} = \begin{bmatrix} 0 & 0 \\ 0 & 0 \\ Y_R(i) & Y_A(i) \\ L_R(i) & L_A(i) \\ N_R(i) & N_A(i) \end{bmatrix} \tag{2}$$

and $\boldsymbol{E} = [0\ 0\ 0\ 0\ 1/I_{zz}(i)]^T$, g is the constant of gravity, $V_{\mathrm{TAS}}(i)$ is true airspeed (TAS), $I_{zz}(i)$ is the moment of inertia about the z axis, and $Y_\beta(i), \ldots, L_\beta(i), \ldots,$ and $N_\beta(i), \ldots$ are the stability derivatives for the lateral forces and moments.[13,14] They depend on continuously varying parameters such as Mach, altitude, angle of attack, weight condition, and wing configuration. Multimodel means that the corresponding, continuous set of state-space models, which arises from these continuous parameter variations, is replaced by a discrete set of state-space models (multimodel set). The index (i) counts the state-space models (representatives) of the multimodel set. Further parameter variations result from design uncertainties, tolerances, and a quasi-static approximation of the structural flexibility.

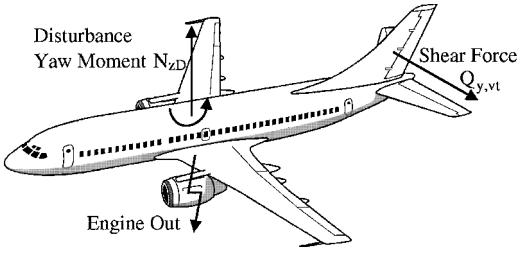

Fig. 1 EO.

III. Requirements

Structural dynamic requirements are as follows:

1) Low lateral load factor n_y at the center of gravity is required, guaranteeing, together with low flight mechanical quantities (see subsequent discussion), a sufficiently low lateral loads level.

2) Adequate performance in loads and stress is required at the vertical tail, that is, in the correlation between shear force $Q_{y,\mathrm{vt}}$ (Fig. 1) and induced torsion moment $M_{z,\mathrm{vt}}$ and between shear force $Q_{y,\mathrm{vt}}$ and induced bending moment $M_{x,\mathrm{vt}}$, abbreviated by phase loads: In case of an EO under a normal flight control situation, sideslip and rudder deflection contributions to $Q_{y,\mathrm{vt}}$ and $M_{x,\mathrm{vt}}$ add up, whereas the contributions to $M_{z,\mathrm{vt}}$ nearly cancel, leaving the fin root with large shear and bending but low torsion. In case of a pilot overreaction, the shear force and the bending moment are increased and the torsion moment is shifted away from the zero line. An EO controller is expected to keep these transients small due to early activation, meaning lower transient and stationary values in sideslip angle and rudder deflection. To avoid a pilot panic reaction, the yaw rate has to be kept low.

The phase loads resulting from an EO are a design driver for the vertical tail, involving considerable effort in structural dynamic assessment. They can bring about considerable extra weight for a large transport AC, arising, for example, from an adequate design of the center box of the vertical tailplane and the rudder attachment structure.

Flight mechanical requirements are as follows:

3) The EO controller has to reduce the magnitudes of the lateral flight mechanical quantities r, β, and p to such an extent that any pilot interference to stabilize the AC after EO is unnecessary.

4) Achieving an early yawing moment compensation by an early drastic rudder deflection also allows to fulfill the requirement for low rolling rates.

5) Small sideslip angle and aileron deflections for minimum drag and optimal slope (in particular in second segment climb) are required.

6) Small lateral displacement and change of heading angle for little course deviation are required.

Requirements concerning control law design are as follows.

7) A simple controller structure is desirable from various viewpoints: costs, reliability, transparency, and simple integration into an existing EFCS.

8) Nonlinearities must be considered in controller design[13] in particular rate and amplitude limitations of actuators (to avoid limit cycles) and nonlinear characteristics of ailerons and spoilers.

9) There must be robust controller performance (cf. Introduction).

IV. Robust Synergetic Design Methodology

The robust synergetic controller design in parameter space consists of three steps:

1) Find different robust controller structures, to fulfill the multidisciplinary requirements.

2) Integrate these controller structures into a common controller structure, termed robust synergetic controller structure.

3) Apply the parameter space method to the synergetic controller structure, to do the compromising between the multidisciplinary requirements and the corresponding design methodologies of the individual controllers and to impose robustness simultaneously.

Concerning step 1, to fulfill loads requirements 1 and 2, the dynamics of the loads, that is, in particular the shear force, at the vertical tail is robustly decoupled from the yawing motion by a dynamic feedback of the yaw rate r to the rudder δ_R:

$$\dot{\delta}_{\mathrm{control}} = k_\psi r + k_{r1}\dot{r} + K_{\mathrm{prefilter}}\delta_{\mathrm{pilot}}, \qquad \delta_R = \delta_{\mathrm{control}} + \delta_{\mathrm{pilot}} \tag{3}$$

The reason for this so-called robust unilateral decoupling controller is that the EO yaw moment N_{zD} has not only an immediate effect on the shear force but also a strong long-term effect via the integration of the yaw rate derivative $\dot{r}$ to the yaw rate r, which then couples to the shear force. Physically speaking, the yaw rate grows rapidly after EO and induces large shear forces. It is this effect that the robust unilateral decoupling controller compensates. Obviously, decoupling of the perturbative yaw rate from the shear force is more efficient than only damping the yaw rate by a conventional lateral controller.

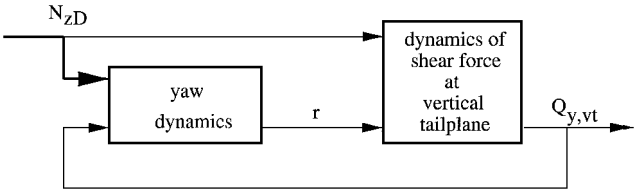

Fig. 2 Bidirectional coupling between the shear force $Q_{y,\mathrm{vt}}$ and the yaw rate r in the flat lateral aircraft motion with a conventional yaw damper in case of an EO.

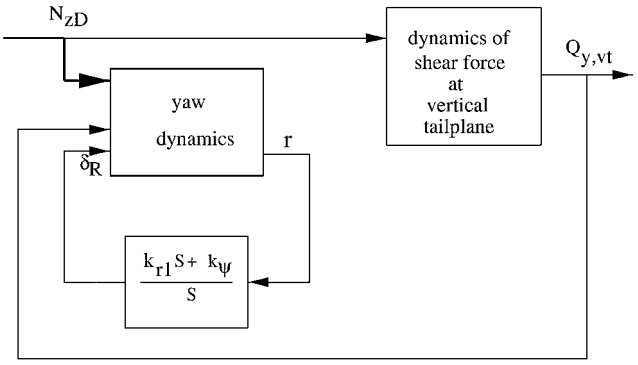

Fig. 3 Robust unilateral decoupling of the shear force $Q_{y,\mathrm{vt}}$ from the yaw rate r in case of an EO by a dynamic feedback of the yaw rate to the rudder, by which the shear force is reduced.

Figures 2 and 3 show the unilateral decoupling controller. When the transfer function from the rudder deflection angle to the shear force at the root of the vertical tail is considered, the controller structure achieves an approximate pole-zero cancellation of the Dutch roll mode. This controller structure is physically and analytically derived in the Appendix. To meet the multidisciplinary requirements 1–5 it is combined with the following lateral controller structure of an SAS:

$$\boldsymbol{u} = \boldsymbol{K}\boldsymbol{x}, \qquad \boldsymbol{K} = \begin{bmatrix} 0 & 0 & k_\beta & 0 & k_{r0} \\ k_\phi & 0 & 0 & k_p & 0 \end{bmatrix} \tag{4}$$

In extension to a standard SAS,[13,14] the sideslip angle β is used as a feedback signal to provide extra freedom in the controller design (see also Ref. 15). As the robust synergetic design refers to feedback design and not to prefilter design, in the following, only the feedback gains will be considered. A prefilter design is not restricted by the robust synergetic controller design and can be accomplished by any method afterward, taking advantage of the achieved robustness.

In the second step, the controller structures (3) and (4) are combined:

$$\boldsymbol{K} = \begin{bmatrix} 0 & k_\psi & k_\beta & 0 & k_r \\ k_\phi & 0 & 0 & k_p & 0 \end{bmatrix}, \qquad k_r = k_{r0} + k_{r1} \tag{5}$$

To avoid a stationary yaw rate, the controller is also designed as a PI–MIMO controller. Now, to achieve such a robust synergetic combination of controller design methods and goals, the parameter space method is used. This approach can be applied to arbitrary controller structures in form of parametric linear time invariant (LTI) systems, arising from combining different controller design methodologies. In the following, first the parameter space method is briefly introduced: The parameter space method allows stabilizing simultaneously an arbitrary, finite number of plants (according to the multimodel approach) with common free parameters $\boldsymbol{q}$, for example, controller parameters $\boldsymbol{q} = \boldsymbol{k}_{\mathrm{con}}$. It is remarkably based on a necessary and sufficient criterion. In particular, not only a fixed controller, but a whole set of controller parameters can be computed for a given controller structure (as an arbitrary LTI system). For flight control, Hurwitz stability is not sufficient. At the same time, good performance does not require an exactly specified location for all eigenvalues. Instead, pole regions are sufficient. This leads to the

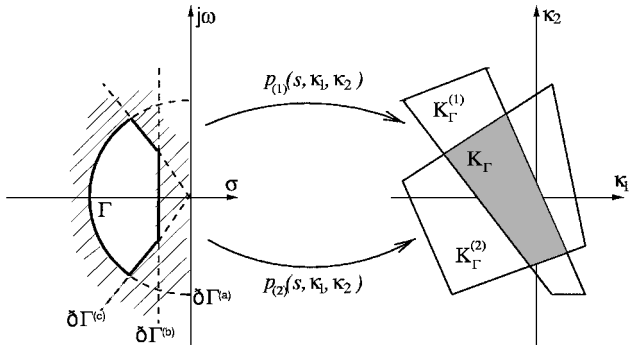

Fig. 4 Parameter space method: simultaneous Γ stabilization for two representatives (within a multimodel approach) in the controller subplane (κ_1 and κ_2).

notion of Γ stability, where Γ describes a subset of the left-half of the complex s plane. This allows considering certain specifications such as settling time (see the boundary $\partial\Gamma^{(c)}$ in Fig. 4), damping ($\partial\Gamma^{(b)}$), and bandwidth ($\partial\Gamma^{(c)}$). A system is called Γ stable if its eigenvalues are entirely contained in the region Γ. Because the region can be arbitrarily shaped, enlarged, and contracted, compromises between different design goals and synergetic combinations of different goals can be found. The problem is now to determine the set of parameters $\boldsymbol{k}_{\mathrm{con}}$, for which, first, the nominal system and, then, the whole multimodel system is Γ stable. To solve it, the parameter space method considers the characteristic polynomials $p_{(i)}(s, \boldsymbol{k}_{\mathrm{con}}), i = 1, \ldots, n_\Sigma$, of a multimodel system such as Σ [Eq. (1)]: First, only one representative or the nominal plant $p_{(1)}(s, \boldsymbol{k}_{\mathrm{con}})$ is considered. The boundary of the region Γ is mapped into a two-dimensional subplane of the $\boldsymbol{k}_{\mathrm{con}}$ space, termed the (κ_1, κ_2) plane, via the characteristic polynomial $p_{(1)}(s, \kappa_1, \kappa_2)$ (see Fig. 4). The simplest plane is chosen via two coordinates of $\boldsymbol{k}_{\mathrm{con}}$, $\kappa_1 = \boldsymbol{k}_{\mathrm{con},i}$ and $\kappa_2 = \boldsymbol{k}_{\mathrm{con},j}$. To compute this mapping, the characteristic polynomial is separated into its real and its imaginary part for an arbitrary grid point $s^* = \sigma^* + j\omega^*$ on the boundary $\partial\Gamma$ of the region Γ. Then the set of equations

$$\mathrm{Re}\, p_{(1)}\left(\sigma^* + j\omega^*, \kappa_1, \kappa_2\right) = 0, \qquad \mathrm{Im}\, p_{(1)}\left(\sigma^* + j\omega^*, \kappa_1, \kappa_2\right) = 0 \tag{6}$$

is solved for κ_1 and κ_2. Solving Eq. (6) along the boundary $\partial\Gamma$ yields the Γ-stability boundaries in the (κ_1, κ_2) plane (see the boundary representation theorem in Ref. 10). These boundaries divide the (κ_1, κ_2) plane into a finite number of regions. By checking Γ stability of an arbitrary point of each region, the set of Γ-stabilizing gains (κ_1, κ_2) can easily be determined. This is based on the boundary crossing theorem[9] constituting a sufficient and necessary condition for Γ stability. Several iterations of the choice of the subplanes may be necessary to achieve the final controller. Here, only two iterations were needed.

In the multimodel case, a controller has to be designed that simultaneously Γ stabilizes all representatives. Therefore, the set of Γ-stabilizing parameters is determined for each representative, and finally, the intersecting set K_Γ is formed (Fig. 4). Controllers out of this intersecting set will Γ stabilize all given representatives.

In the third step the parameter space method is applied to the robust controller structure. The multimodel Σ [Eq. (2)] yields the set of parametric characteristic polynomials of the closed-loop system:

$$p_{(i)}(s, \boldsymbol{k}_{\mathrm{con}}) = \det\left(s\boldsymbol{I} - \boldsymbol{A}_{(i)} - \boldsymbol{B}_{(i)}\boldsymbol{K}\right), \qquad i = 1, \ldots, n_\Sigma$$
$$\boldsymbol{k}_{\mathrm{con}} = [k_\psi, k_\phi, k_\beta, k_p, k_r] \tag{7}$$

To fulfill the multidisciplinary requirements, in particular requirements 3 and 4, the Γ regions are chosen according to Fig. 5. For the Dutch roll mode, two symmetric (with respect to the real axis) pineapple segments are chosen. The straight parts $\partial\Gamma^{(1)}$ and $\partial\Gamma^{(2)}$ of the boundary guarantee sufficient damping and avoid overdamping or even the complex poles to merge to two real poles. The circular parts $\partial\Gamma^{(3)}$ and $\partial\Gamma^{(4)}$ ensure a sufficiently fast response and avoid high gain controllers, which cause too high roll frequencies. For

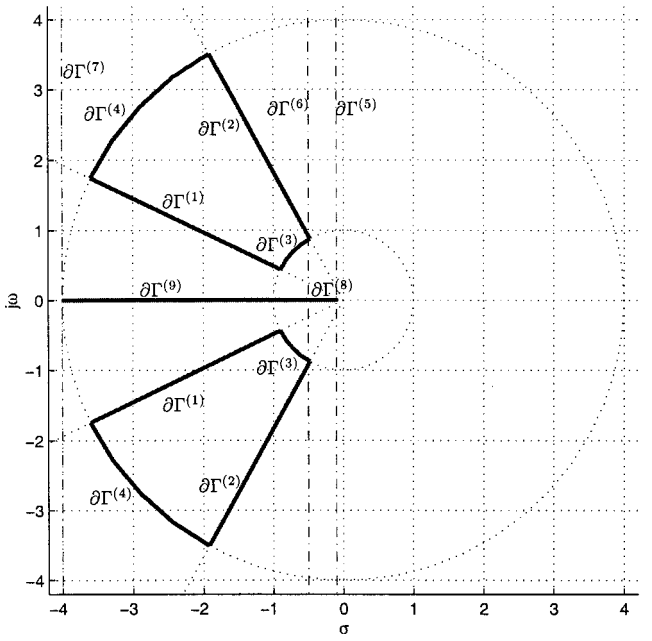

Fig. 5 Chosen Γ regions: unification of bounded sets in the complex *s* plane, specifying the dynamic requirements for the closed-loop system; bold face lines of $\partial\Gamma^{(8)}$ and $\partial\Gamma^{(9)}$ specify branch point avoidance.

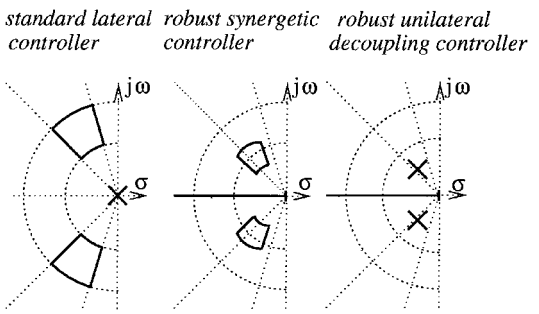

Fig. 6 Synergetic controller design in terms of Γ regions for the Dutch roll mode and the controller mode.

the real poles, real boundaries $\partial\Gamma^{(5)}$, $\partial\Gamma^{(6)}$, and $\partial\Gamma^{(7)}$ bring about sufficient disturbance rejection and sufficient rolling performance. The chosen intervals are $[-4, -0.5]$ for the roll mode and $[-0.4, -0.1]$ for the spiral mode. The boundary at -0.1 also applies to the additional controller pole from integrating the yaw rate (controller mode).

However, branch points, that is, merging of two real poles to a complex conjugate pole pair, have to be avoided to transfer the physical interpretation of each eigenvalue from the open-loop to the closed-loop system. A branch point is characterized by a simultaneous zero of the characteristic polynomial and its derivative. This condition induces an extra boundary in parameter space (branch point avoidance boundary).

Via the pineapple segment and the first interval $[-0.4, -0.1]$, the robust synergetic combination of the lateral controller structure [Eq. (4)], the robust unilateral decoupling controller, and the PI–MIMO controller can be adjusted (Fig. 6):

1) If the pineapple segments and the pole positions within the pineapple segment move toward the corresponding zeros of the disturbance transfer function, the robust unilateral decoupling controller and the robust closed-loop dynamics thereby induced become more dominant.

2) If the real boundary is lowered toward the origin, the additional controller pole moves to zero and the dynamic characteristics of the lateral controller structure [Eq. (4)] become more dominant.

3) If this boundary and the additional controller pole move in opposite directions, the robust disturbance rejection via the PI controller becomes more dominant.

It has to be emphasized that synergetic robustness is not only a property of the controller structure, but is also imposed by lowering dynamic requirements via Γ regions and considering parameter variations via the multimodel approach.

In the following, the design steps for the structural dynamic EO controller are described. As a first design step, the damping of the Dutch roll mode is robustly increased via k_β and k_r. A root loci, a controllability, and an observability analysis[13] reveal that these gains have only a little or a moderate influence on the other poles, that is, roll, spiral, and additional control mode. When the parameter space method is considered, the complex equation in k_r and k_β

$$p_{(i)}(s, \boldsymbol{k}_{\text{con}}) = 0, \qquad i = 1, \ldots, n_{\text{critical}} \tag{8}$$

with fixed parameters $k_\phi = 0, k_p = 0$, and $k_\psi = 0$; $s \in \partial\Gamma^{(j)}$, $j = 1, \ldots, n_\Gamma$, has to be solved for all s belonging to the n_Γ Γ-region boundaries for all n_{critical} critical representatives. These critical representatives are 11 load cases for the lowest velocity at zero altitude, chosen by comparative simulations from the multimodel set. This yields the Γ-stability boundaries in the k_β–k_r plane (see Fig. 7; for transparency, here only one critical representative is considered). The computation of the Γ-stability boundaries have been carried out using Paradise, a new MATLAB® toolbox for robust parametric control design.[‡] Because roll, spiral, and controller modes are not considered in this step, but will be considered in the following design steps, the corresponding Γ regions have been enlarged toward the origin, still guaranteeing stable behavior. Therefore, the Γ-stabilizing set of controllers is only restricted as a consequence of the Γ region for the Dutch roll mode (Fig. 7).

The gains are chosen as $k_r = 5$ and $k_\beta = -5.2$ (see asterisk in Fig. 7). This choice is both sufficiently small (in particular concerning the rate limitation of the rudder) and sufficiently far away from the stability boundaries for an adequate robust performance. In the second step the complex equation

$$p_{(i)}(s, \boldsymbol{k}_{\text{con}}) = 0, \qquad i = 1, \ldots, n_{\text{critical}} \tag{9}$$

with fixed parameters $k_\beta = -5.2$, $k_r = 5$, $k_\psi = 0$, and $s \in \partial\Gamma^{(j)}$, $j = 1, \ldots, n_\Gamma$, is now solved for k_ϕ and k_p. The preceding enlargement of the Γ regions (Fig. 5) is withdrawn. The gains are chosen according to the same arguments as in the preceding step. In the final step,

$$p_{(i)}(s, \boldsymbol{k}_{\text{con}}) = 0, \qquad i = 1, \ldots, n_{\text{critical}} \tag{10}$$

with fixed parameters $k_\phi = 1, k_p = 1.5, k_\beta = -5.2$, and $s \in \partial\Gamma^{(j)}$, $j = 1, \ldots, n_\Gamma$, has to be solved for k_ψ and k_r (Fig. 8). This step also constitutes a first assessment by considering all relevant low-velocity cases combined with critical weight conditions within the multimodel approach. It is an essential advantage of the method not to restrict the number of representatives, that is, the same number can be considered within the controller design as in the final assessment of the controller. Therefore, a worst-case analysis becomes unnecessary. The permissible set of simultaneous Γ-stabilizing controllers is the accentuated parallelogram, from which the controller is chosen (see asterisk in Fig. 8). The set is generated by both the complex and the real boundaries, originating from different representatives. Choosing the final parameters from this permissible set can now be done by imposing additional or stricter requirements or iterative (simulative) analysis, also involving modified Γ regions. Figure 9 shows the consequence of lowering the requirement of robust quasi-exact pole-zero cancellation (as indicated in Fig. 6) toward a robust synergetic controller, also having characteristics of a PI controller: The early slope up to 1 s in the lateral acceleration n_y and the long-term performance (above 2.5 s) of n_y, yaw rate r, and bank angle ϕ are improved by the synergetic controller, whereas the early performance (0.3–2.5 s) of n_y and r becomes worse, resulting in transient peaks that are increased by about 30%. (Note that quasi exact means that, for robustness via fixed controller gains, the strict requirement of a simultaneous exact pole-zero cancellation for all models has been lowered toward an approximate pole-zero cancellation.)

[‡]URL: http://www.op.dlr.de/FF-DR-RR/paradise.

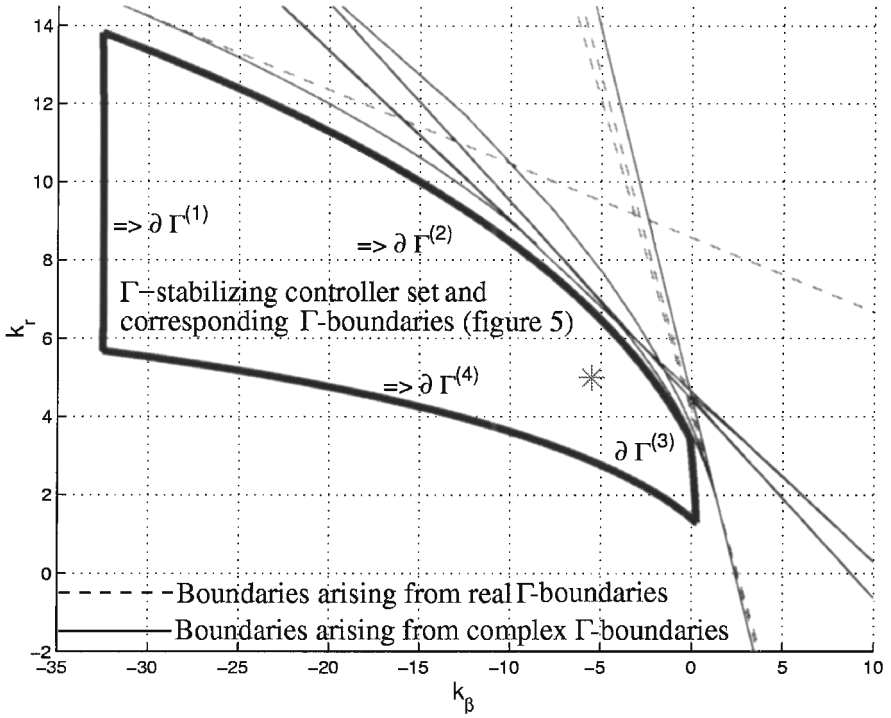

Fig. 7 Γ-stability boundaries in k_β–k_r plane for one critical representative at low velocity and low altitude.

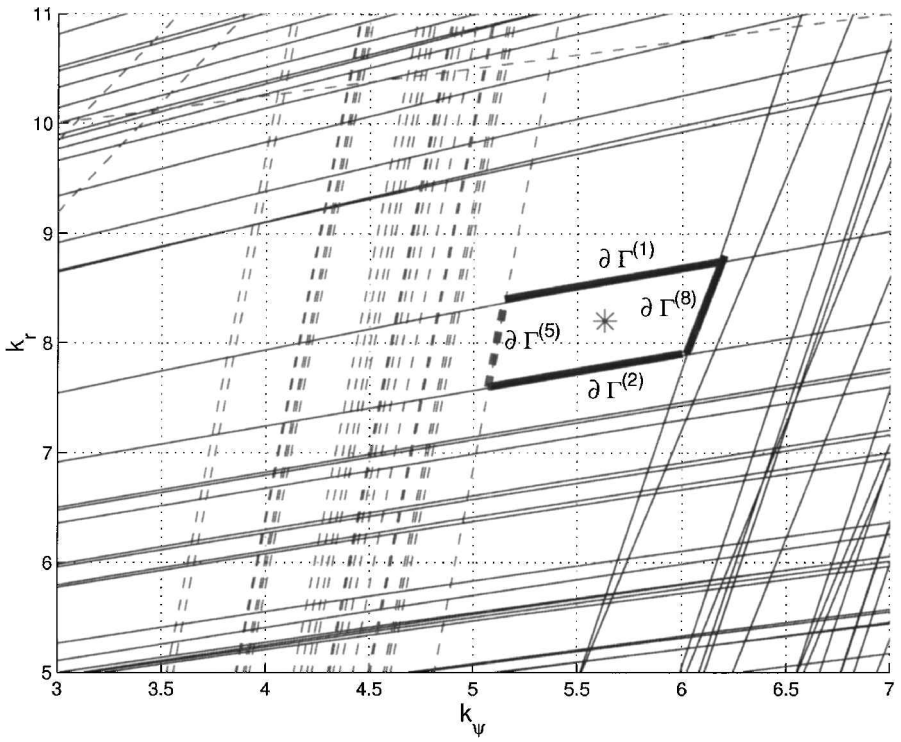

Fig. 8 Zoomed Γ-stability boundaries in k_ψ–k_r plane for 11 critical load cases for Mach = 0.2 and 0.35 and zero altitude; corresponding Γ regions given in Fig. 5. The relevant inner boundaries (in bold) correspond to different load cases.

V. Analysis of Controller Performance

For analysis, the robust synergetic controller has to be compared with a standard lateral controller of a standard EFCS in the normal law controller mode,[6] in the following abbreviated by the normal law.[6] The EO is simulated as a worst case, that is, the thrust of the critical engine is reduced in the form of a step from maximum thrust to zero (Fig. 10). This corresponds to a burst or the initial dynamics in case of a mechanical failure[3] and yields a quicker loss in thrust than the case of a very simple first-order modeling of the engines.[3,6]

For structural dynamic analysis, a pilot panic reaction as specified in JAR 25.367 has to be superimposed on the control surface deflection commands from the normal law. It is illustrated by the corresponding rudder deflection angle in Fig. 10. It does not takes place before the maximal yaw rate is reached and not earlier than 2 s as a worst case in pilot reaction time.[2] It consists of a drastic rudder command, even up to the rudder travel limitation (RTL) and to the rudder rate limitation, that is, the pilot pushes the pedals to the stops as quickly as possible. Although not required in JAR 25.367, the maximal rudder deflection rate is held for up to 0.5 s. When the RTL or a deflection close to the RTL is reached, the rudder is kept there for up to 1 s. Then, on feeling a significant reduction in the yaw rate, the pilot will instantaneously reduce the

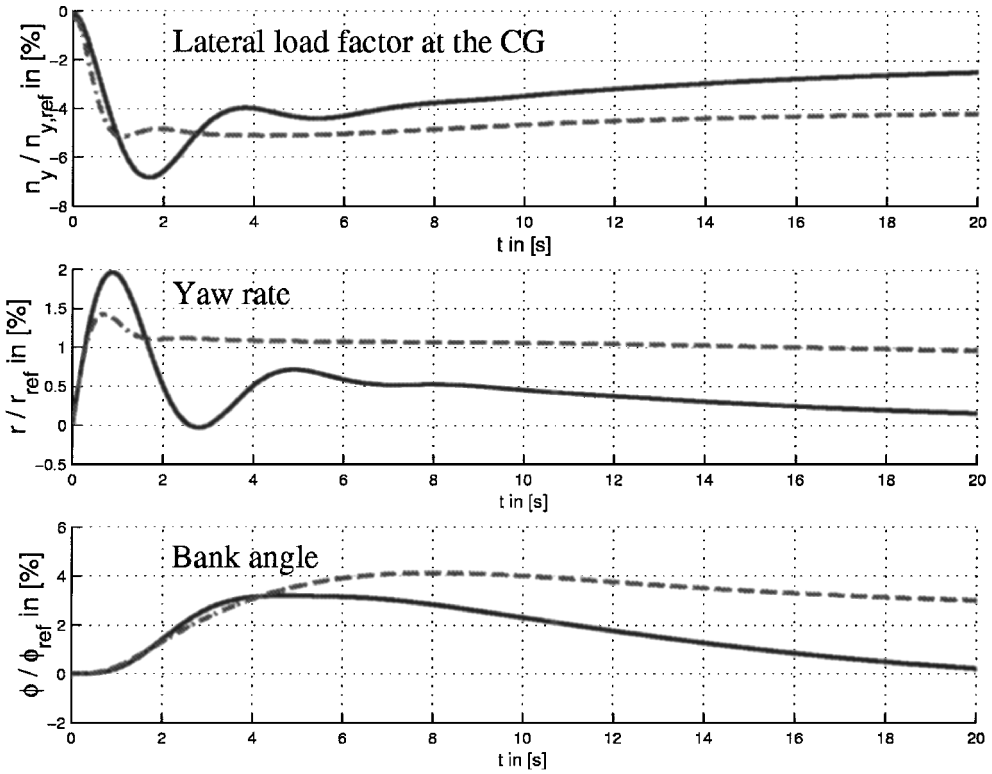

Fig. 9 Comparison of the synergetic robust controller (solid line) and the robust unilateral decoupling controller (dashed line) in a critical EO situation.

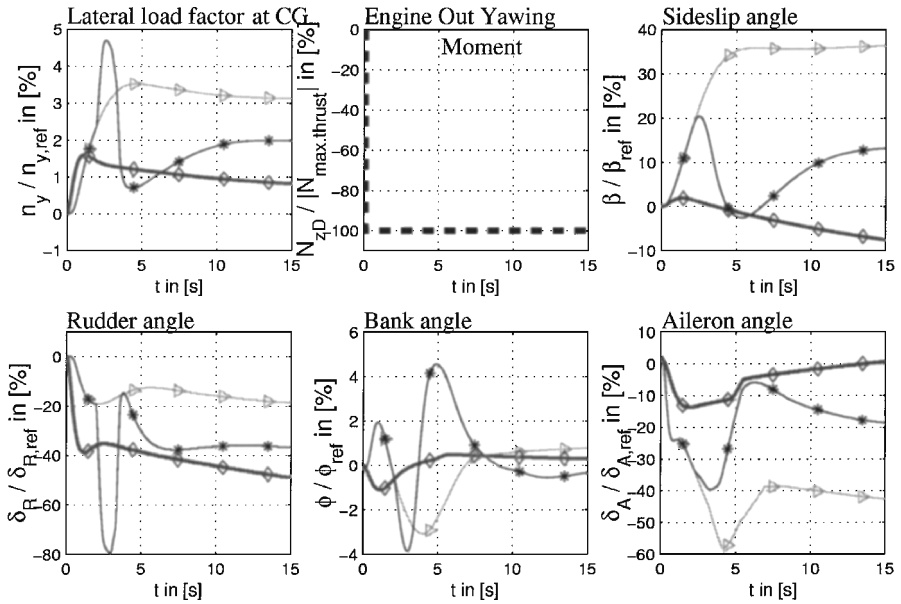

Fig. 10 Comparison of the normal law (▷), the normal law + pilot (∗), and the synergetic EO controller switched on after a detection time <100 ms (◇) in a critical EO situation.

rudder deflection to half its value. Afterwards, rudder and aileron deflections are used to achieve a stationary state, so that the pilot can establish the optimal sideslip angle and stabilize the flight path. This case is abbreviated as normal law + pilot. Simulations are performed on a nonlinear high-precision model, which has the following characteristics: 1) complete nonlinear differential equations for rigid-body motion, 2) detailed nonlinear aerodynamic model, 3) structural flexibility, approximated by flexible factors, 4) corrections from unsteady aerodynamics, 5) nonlinear actuator and EFCS modeling, and 6) additional tolerances, describing early design uncertainties.

In the flight envelope, low altitudes and low velocities are the most critical cases in an EO situation. To show robustness, Mach = 0.2 and 0.35 and 11 critical load cases are considered. The analysis of lateral maneuvers in combination with an EO is exemplified by a steady turn for the preceding load cases at zero altitude, which is a conservative requirement in structural dynamics, and for Mach = 0.2. Additional tolerances in the derivatives up to 20% are simultaneously considered.

A. Structural Dynamic and Robustness Analysis

A first indicator for a sufficient dynamic performance is the lateral load factor n_y at the c.g. The first transient peak is reduced by 60% compared to the normal law + pilot and by 50% compared to the normal law (Fig. 10). In stationary values, there is a reduction of more than 30% (normal law) and of 50% (normal law + pilot), indicating the advantages of an early drastic compensation.

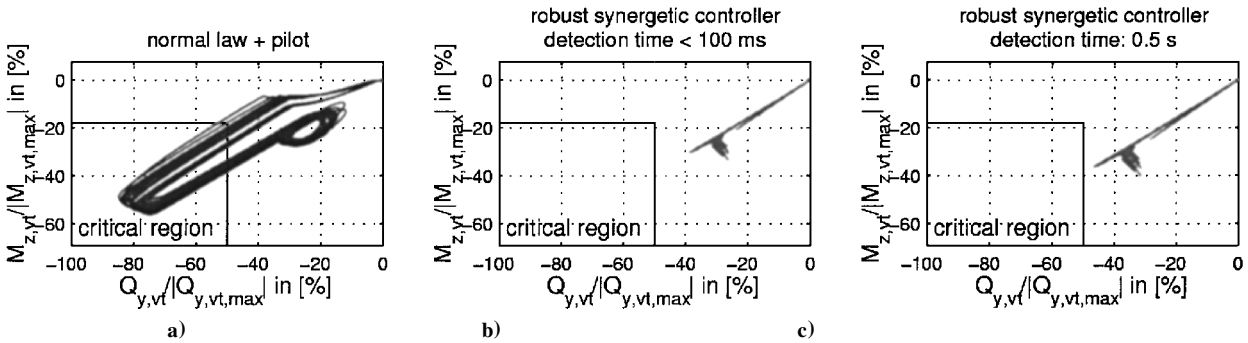

Fig. 11 Phase load diagram for the vertical tailplane for 11 load cases at Mach = 0.2 and 0.35 at zero altitude.

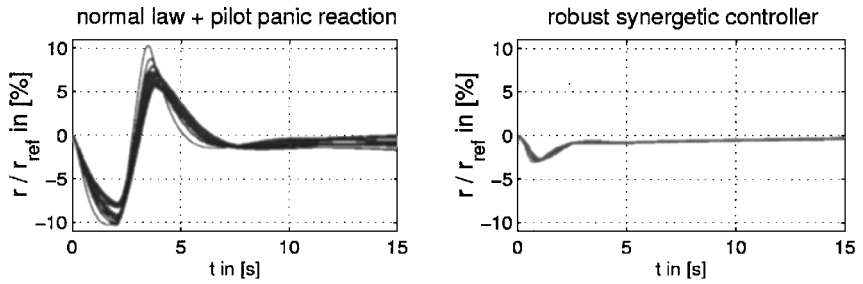

Fig. 12 Time histories of the yaw rate r for 11 load cases at Mach = 0.2 and 0.35 at zero altitude.

In structural dynamics and in statics, the shear force at the vertical tail $Q_{y,vt}$ and the corresponding bending and torsion moments, $M_{x,vt}$ and $M_{z,vt}$, at the root of vertical tail are analyzed in phase load diagrams (Fig. 11). Critical operational states are here shown as regions. In contrast to the flight mechanical coordinate system, a local coordinate system of the vertical tail is used. [Compared to the flight mechanical coordinate system, the x and the z axes are inverted and rotated about the y axis (by the sweep angle of the vertical tail) so that the z axis is parallel to the elastic axis of the vertical tail.] Figure 11 compares the robust synergetic EO controller (Figs. 11b and 11c) with the normal law + pilot (Fig. 11a). Two detection times for the EO are considered: a time less than 100 ms (Fig. 11b) and a time of 0.5 s (Fig. 11c). After the detection time, the EO controller is switched on with full authority. Figure 11 indicates that the regions of simultaneous large shear force and torsion moment are robustly avoided as a result of using the EO controller. The extreme values of the shear force and the torsion moment are almost halved by the EO controller.

In more detail, the synergetic controller reduces the transient peaks of the shear force by more than 50% (normal law + pilot). The stationary values are reduced by 50% compared to the normal law + pilot. When the torsion moment $M_{z,vt}$ is considered, the synergetic controller reduces the transient peak (normal law + pilot) by 55% and brings about a much better performance in transients than the normal law + pilot. This is a consequence of the achieved reduction in sideslip angle (Fig. 10) showing the interplay between flight mechanics and structural dynamics.

The achieved robustness is remarkable, that is, the area covered by the set of all phase curves, resulting from different flight and weight conditions, is nearly condensed to one curve (Figs. 11b and 11c). For static analysis, this implies significantly reduced work in assessment. Moreover, for future large AC, the vertical tail can be lighter (cf. Sec. III) than for today's AC as a result of the EO controller.

B. Flight Mechanical and Robustness Analysis

In contrast to the normal law and the normal law + pilot, the robust synergetic controller avoids large magnitudes in transient and final states (Fig. 10), that is, large maneuvers in consequence of EO, so that any pilot interference becomes unnecessary. This is achieved by an immediate and efficient rudder command, nearly reaching the final rudder angle for the yawing moment compensation after 1 s. Therefore, the engine failure is fully compensated, that is, the airplane is in a nearly stationary state after 1 s, which is 50% of the pilot's reaction time according to JAR 25.367. Additionally, the commanded rudder rate is lower than that in case of the normal law + pilot. Delays in the yawing moment compensation result in more energy being transferred to the rolling motion. Consequently, more aileron activity is necessary to compensate this effect.

Concerning the flight mechanics quantities in more detail, the following improvements can be observed:

1) The yaw rate r is reduced by 60% in transient peaking compared to the normal law and the normal law + pilot (Fig. 12). After 1 s the yaw acceleration already changes its sign, so that there will be no reason for any pilot interference (see requirement 3 of Sec. III). In consequence of the PI controller design, the yaw rate goes to zero sufficiently quickly. Therefore, only little deviations will occur in heading in contrast to the normal law and the normal law + pilot (see requirement 6).

2) The transient peak in bank angle ϕ (Fig. 10) is reduced by 30% (normal law + pilot) and by 10% (normal law), which means significantly improved passenger comfort.

3) The peak in aileron angle δ_A is reduced by 60% compared to the normal law + pilot and by 80% compared to the normal law (Fig. 10). Correspondingly, the spoiler deflections in case of the synergetic controller are negligible, whereas, in the other cases, the deflection angles are three times higher (normal law) and four times higher (normal law + pilot).

4) The sideslip angle β (Fig. 10) is reduced in transient peaking by more than 90% and in its final value by 40% (normal law + pilot) and 150% (normal law), which, combined with the achieved yawing performance, guarantees a significantly lower lateral deviation from the flight path (see requirement 6). Taking low aileron deflections into account, the drag will be significantly reduced (see requirement 5). Note that this performance was achieved with a very simple controller structure (see requirement 7).

Figures 11 and 12 indicate that the robustness of the normal law is even increased by the EO controller (see requirement 9). The amplitude variations of the ensemble of the yaw rate time histories in the first peak, which are generated by parameter variations, are reduced by more than 50% by the robust synergetic EO controller. In Fig. 13, the EO controller is extended from a SAS to a standard CSAS for turn coordination.[13] It allows the pilot to interfere at any

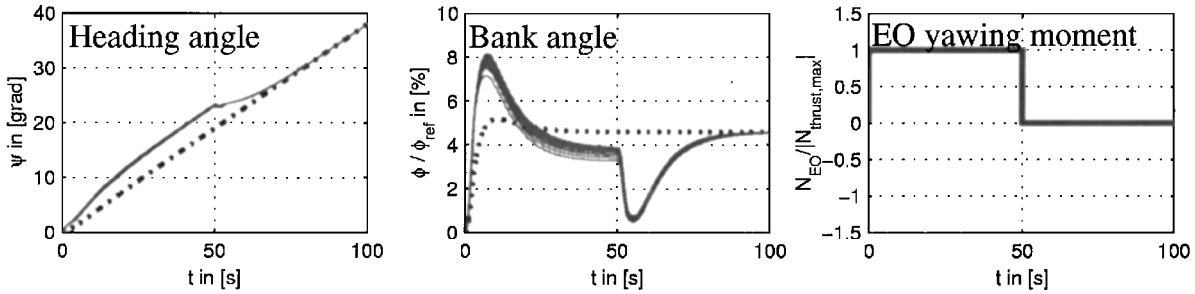

Fig. 13 Steady turn in combination with an EO for 11 load cases at Mach = 0.2 and 0.35 at zero altitude: robust synergetic controller (solid line) and AC dynamics without EO (dotted line).

time after the EO and has a very robust performance as argued in the Introduction (robustness of a CSAS has to be achieved by its feedback part, that is, the SAS). Figure 13 shows an EO at the very beginning of a turn. Although the dead engine was chosen in such a way that the yawing moment for the turn is enforced by the EO yawing moment, no critical flight condition arises. Only small deviations from the commanded values occur in heading and bank angle. These deviations vanish completely after the engine has been restarted. Therefore, the CSAS allows the pilot to do or continue maneuvers in spite of the EO and has a robust automatic reconfiguration property. In other words, the workload of the pilot in case of an EO is reduced.

In spite of considering extra design uncertainties, for example, rudder effectiveness, and changing the matrix entries of Eq. (1) up to 20%, the robust design methodology still allowed to account for them. All assumptions in controller design, concerning nonlinearities (requirement 9) are fulfilled. 1) Low rates and rotational angles are achieved, guaranteeing little corrections from gyroscopic and gravity terms and nonlinear aerodynamics. 2) There are low aileron angles (Fig. 10), avoiding nonlinear aileron–spoiler gearing and nonlinear aerodynamics of ailerons and spoilers. 3) The gains have been selected sufficiently low so that the commanded values avoid rate and amplitude limitations. Consequently, limit cycles will not occur.

It is remarkable that robustness has been achieved in spite of some unmodeled dynamics, for example, sensor and filter dynamics and discrete data processing. Therefore, it was decisive that all controller parameters were chosen in such a way that their distance to the Γ-stability boundaries in parameter space was maximal (cf. Figs. 7 and 8) and that the Γ regions have a certain distance from the imaginary axis.

VI. Conclusion

Based on Ackermann's[10] parameter space method, a new method for the robust combination of different types of LTI controller structures and for finding compromises between multidisciplinary targets has been developed. It is applied to the design of a structural dynamic EO controller. The controller is compatible with flight mechanical and HQ requirements. The perturbations of the lateral motion in consequence of the EO are reduced to such an extent that no pilot interference for the yawing moment compensation and stabilization is necessary. The effect of the flight dynamics on the loads at the vertical tail is reduced because the EO controller approximately achieves a robust unilateral decoupling of the shear force at the vertical tail from the yawing rate. Consequently, the loads at the vertical tail and thereby the costs for its design and its assessment are significantly reduced.

Simultaneously, a new type of pilot assistance system has been demonstrated. It is characterized by a very early interference within human reaction time: Obviously, an automatic system can master critical situations in a much better way by avoiding reaction time delays and overreaction. Instead of first letting the aircraft drift into an extreme flight situation, which then is hard to master, the early yaw moment compensation keeps the aircraft in a moderate flight condition. Consequently, a delayed overreaction of the pilot is prevented. The pilot has enough time for the operation of the engines and for returning to the original flight path. Thereby, a task separation is achieved, which enables the pilot to concentrate on planning and performing long-term tasks. The short-term tasks, in particular within the reaction time of the pilot, are performed by the automatic system. For a standard command system, it was demonstrated that, in case of an EO, the pilot can perform a turn in the conventional way. Simultaneously, the quick EO yawing moment compensation is achieved by the automatic assistance system. Consequently, at any time the pilot has full authority to perform any maneuver.

In simulations on a nonlinear model, the design of the EO controller as a SAS and the design as a CSAS turned out to be very robust with regard to any parameter variations (flight envelope, weight condition, early design uncertainties) and to nonlinearities. Such a robustness was achieved because the method is based on a necessary and sufficient criterion for Γ stability, which allows to consider many flight cases arbitrary for the controller design.

The design method and the resulting controller structure are simple and physically transparent. The procedure provides a new analytical approach to find compromises between multidisciplinary requirements and corresponding controller structures given as LTI systems. It appears to be feasible for other multidisciplinary aircraft control problems such as maneuver load alleviation or structural mode control.

Appendix: Derivation of the Robust Unilateral Controller Structure

The shear force $Q_{y,\mathrm{vt}}$ at the vertical tail mainly consists of the aerodynamic force $F_{y,\mathrm{tail}}$ at the vertical tail and the inertia force corresponding to the lateral acceleration $a_{y,\mathrm{tail}}$ at the vertical tail.[3] To meet all requirements (cf. Sec. III), the controller has not only to balance both contributions but also has to ensure that both are kept small. Simultaneously, the controller has to balance all yawing moments. These goals have to be achieved robustly, that is, for all flight and weight conditions.

In the following, it is justified and derived that a robust approximate decoupling of both the lateral acceleration and the lateral aerodynamic force at the vertical tail is suited to meet the requirements at an adequate level.

The yawing moment of the engine failure and the rudder deflection essentially occur in the flat lateral motion[3] so that Eq. (1) can be simplified:

$$\begin{bmatrix}\dot{\beta}\\ \dot{r}\end{bmatrix}=\begin{bmatrix}Y_\beta & Y_r-1\\ N_\beta & N_r\end{bmatrix}\begin{bmatrix}\beta\\ r\end{bmatrix}+\begin{bmatrix}Y_{\delta_R}\\ N_{\delta_R}\end{bmatrix}[\delta_R]+\begin{bmatrix}0\\ 1/I_{zz}\end{bmatrix}[N_{zD}] \quad \text{(A1)}$$

A design goal is to keep the energy transfer from the yaw motion into the roll motion small. If this goal will be achieved later, then this is an a posteriori justification for using this flat lateral model [Eq. (A1)] to derive the controller structure.

Within this flat lateral model, forces and torques are represented by a pair of forces $F_{y,\mathrm{wfp}}$, and $F_{y,\mathrm{tail}}$ (cf. Fig. A1). $F_{y,\mathrm{wfp}}(\boldsymbol{x})$ is the sum of the aerodynamic lateral forces at the wings, the fuselage, and the pods. It depends on the state $\boldsymbol{x}=[\beta\ \ r]^T$ of the aircraft and has a lever arm ℓ_{wfp} with respect to the c.g. $F_{y,\mathrm{tail}}(\boldsymbol{x}, \delta_R)$ is the sum of the aerodynamic lateral forces at the tail, cf. Fig. A1. It depends on both the state $\boldsymbol{x}$ and the input δ_R of the system; its lever arm is ℓ_{tail}.

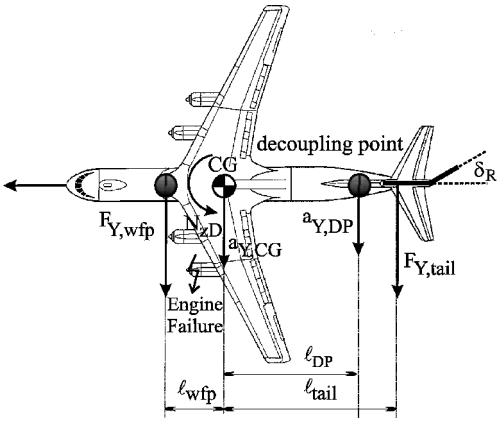

Fig. A1 Definition of DP.

Ideally, the desired balance of yawing moments would be achieved by choosing the rudder deflection angle δ_R such that

$$F_{y,\mathrm{wfp}}(\boldsymbol{x})\ell_{\mathrm{wfp}} - F_{y,\mathrm{tail}}(\boldsymbol{x}, \delta_R)\ell_{\mathrm{tail}} + N_{zD} = 0 \tag{A2}$$

The forces and the disturbance N_{zD} in the yawing moment are unknown, however, so that a robust implementation of the control law (A2) is impossible.

An alternate approach is to split the vehicle dynamics robustly into two subsystems. A first-order subsystem with output lateral acceleration should not be influenced by the yaw rate because the disturbance N_{zD} in the yawing moment primarily enters into the yaw acceleration and rate. A simple choice would be the lateral acceleration at the c.g. Concerning shear force alleviation, the lateral acceleration at the vertical tail should be chosen. In both cases, the yaw rate r as part of the state $\boldsymbol{x}$ enters into the considered lateral acceleration via both unknown forces $F_{y,\mathrm{wfp}}(\boldsymbol{x})$ and $F_{y,\mathrm{tail}}(\boldsymbol{x}, \delta_R)$, and again robustness cannot be achieved. Therefore, we first define a decoupling point (DP) in a distance ℓ_{DP} from the c.g. such that $F_{y,\mathrm{wfp}}(\boldsymbol{x})$ does not enter into the lateral acceleration $a_{y,\mathrm{DP}}$ at the DP (cf. Fig. A1). It is calculated from the condition

$$\begin{aligned} a_{y,\mathrm{DP}} &= a_{y,\mathrm{cg}} - \ell_{\mathrm{DP}}\dot{r} \\ &= (F_{y,\mathrm{wfp}} + F_{y,\mathrm{tail}})/m - \ell_{\mathrm{DP}}(F_{y,\mathrm{wfp}}\ell_{\mathrm{wfp}} - F_{y,\mathrm{tail}}\ell_{\mathrm{tail}} + N_{zD})/I_{zz} \\ &= F_{y,\mathrm{wfp}}(1/m - \ell_{\mathrm{DP}}\ell_{\mathrm{wfp}}/I_{zz}) + F_{y,\mathrm{tail}}(1/m + \ell_{\mathrm{DP}}\ell_{\mathrm{tail}}/I_{zz}) \\ &\quad - (\ell_{\mathrm{DP}}N_{zD})/I_{zz} \end{aligned} \tag{A3}$$

where m is the mass of the AC. The factor of $F_{y,\mathrm{wfp}}$ is zero for

$$\ell_{\mathrm{DP}} = I_{zz}/(m\ell_{\mathrm{wfp}}) \tag{A4}$$

and this choice of ℓ_{DP} yields

$$a_{y,\mathrm{DP}} = F_{y,\mathrm{tail}}(\boldsymbol{x}, \delta_R)(\ell_{\mathrm{wfp}} + \ell_{\mathrm{tail}})/(m\ell_{\mathrm{wfp}}) - N_{zD}/(m\ell_{\mathrm{wfp}}) \tag{A5}$$

Equation (A4) corresponds to a representation of the mass and the moment of inertia by two masses in the positions with the distances ℓ_{wfp} and ℓ_{DP} from the c.g. (Fig. A1). The position of the DP is close to the tail. It is little dependent on the weight condition. Therefore, $a_{y,\mathrm{DP}}$ constitutes an approximation of the lateral acceleration at the vertical tail. In the present paper, however, we assume that ℓ_{DP} is known.

A quantitative analysis of Eq. (A5) for typical AC data shows that the disturbance N_{zD} in the yawing moment resulting from the engine failure has a moderate immediate effect on $a_{y,\mathrm{DP}}$ and a strong long term effect via the integration of $\dot{r}$, where r is a component of the state vector $\boldsymbol{x}$. Physically speaking, the yaw rate r grows rapidly after EO and induces a large acceleration $a_{y,\mathrm{DP}}$ and large shear forces at the root of the vertical tailplane. It is this dominating effect that we want to compensate.

A crucial step for deriving a robust controller structure is that we make $F_{y,\mathrm{tail}}(\boldsymbol{x}, \delta_R)$ independent of the yaw rate r by an appropriate choice of the rudder angle δ_R. The standard linear approach of aerodynamics, resulting from a nonlinear trimming computation and linearization at the trimming point and restricted to the flat lateral motion, yields

$$F_{y,\mathrm{tail}}(\beta, r, \delta_R) = m V_{\mathrm{TAS}}\left(Y_{\beta,\mathrm{tail}}\beta + Y_{r,\mathrm{tail}}r + Y_{\delta_R}\delta_R\right) \tag{A6}$$

The rudder angle is composed of a reference part δ_{pilot} and a feedback part $\delta_{\mathrm{control}}$, that is,

$$\delta_R = \delta_{\mathrm{pilot}} + \delta_{\mathrm{control}} \tag{A7}$$

Consequently, the feedback part $\delta_{\mathrm{control}}$ has to ensure that in the closed-loop system the dynamic equation of $F_{y,\mathrm{tail}}$ does not depend on the yaw rate, that is, it should have the general form

$$\dot{F}_{y,\mathrm{tail}} = f(F_{y,\mathrm{tail}}, \delta_{\mathrm{pilot}}, \dot{\delta}_{\mathrm{pilot}}, N_{zD}) \tag{A8}$$

By assumption, a controller structure of first order is considered:

$$\dot{\delta}_{\mathrm{control}} = k_\psi r + k_{r1}\dot{r} + K_{\mathrm{prefilter}}\delta_{\mathrm{pilot}} \tag{A9}$$

where, k_{r1} is introduced because the aircraft has also a feedback k_{r0} of the yaw rate r to the rudder deflection angle δ_R as a part of the standard lateral controller [Eq. (4)]. In Eq. (5) they are combined: $k_r = k_{r0} + k_{r1}$ and then designed according to the robust synergetic controller design in parameter space. Remarkably, the controller (A9) is restricted to the feedback path of the yaw rate to the rudder, which is the most reliable path in lateral control. Now, differentiating Eq. (A6) and then substituting $\dot{\beta}$, $\dot{r}$, and $\dot{\delta}_R$ by the expressions of Eqs. (A7), (A9), and (A1) yield

$$\begin{aligned} \dot{F}_{y,\mathrm{tail}} = m V_{\mathrm{TAS}}\Big[&\left(Y_{\delta_R}k_\psi - Y_{\beta,\mathrm{tail}}\right)r + \left(Y_{\delta_R}k_{r1} + Y_{r,\mathrm{tail}}\right)(\ell_{\mathrm{wfp}}F_{y,\mathrm{wfp}} \\ &- \ell_{\mathrm{tail}}F_{y,\mathrm{tail}} + N_{zD})/I_{zz} + Y_{\beta,\mathrm{tail}}(F_{y,\mathrm{wfp}} + F_{y,\mathrm{tail}})/(m V_{\mathrm{TAS}}) \\ &+ Y_{\delta_R}(K_{\mathrm{prefilter}}\delta_{\mathrm{pilot}} + \dot{\delta}_{\mathrm{pilot}})\Big] \end{aligned} \tag{A10}$$

Then requiring the terms in r and $F_{y,\mathrm{wfp}}$ to vanish allows the derivation of closed expressions for the controller parameters symbolically:

$$k_\psi = Y_{\beta,\mathrm{tail}}/Y_{\delta_R}, \qquad k_{r1} = -1/Y_{\delta_R}[(\ell_{\mathrm{DP}}Y_{\beta,\mathrm{tail}}/V_{\mathrm{TAS}}) + Y_{r,\mathrm{tail}}] \tag{A11}$$

showing that the choice of controller structure was adequate. Changing coordinates makes the unilateral decoupling more evident. The yaw rate and the controller dynamics

$$\begin{aligned} \begin{bmatrix} \dot{r} \\ \dot{\delta}_{\mathrm{control}} \end{bmatrix} &= \begin{bmatrix} a_{22} & a_{23} \\ a_{32} & a_{33} \end{bmatrix}\begin{bmatrix} r \\ \delta_{\mathrm{control}} \end{bmatrix} + \begin{bmatrix} a_{21} \\ a_{31} \end{bmatrix}[a_{y,\mathrm{DP}}] \\ &\quad + \begin{bmatrix} b_{21} & b_{22} \\ b_{31} & b_{32} \end{bmatrix}\begin{bmatrix} \delta_{\mathrm{pilot}} \\ \dot{\delta}_{\mathrm{pilot}} \end{bmatrix} + \begin{bmatrix} e_{21} \\ e_{31} \end{bmatrix}[N_{zD}] \end{aligned}$$

still depend on $a_{y,\mathrm{DP}}$, but the dynamics of the lateral acceleration at the DP

$$[\dot{a}_{y,\mathrm{DP}}] = [a_{11}][a_{y,\mathrm{DP}}] + [b_{11} \quad b_{12}]\begin{bmatrix} \delta_{\mathrm{pilot}} \\ \dot{\delta}_{\mathrm{pilot}} \end{bmatrix} + [e_1 \quad e_2]\begin{bmatrix} N_{zD} \\ \dot{N}_{zD} \end{bmatrix} \tag{A12}$$

is robustly unilaterally decoupled from the yaw rate dynamics and the controller dynamics. The system matrices can easily be estimated from Eqs. (A1), (A4), and (A6).

Now, the following has been achieved. The lateral acceleration at the DP has been robustly decoupled from the yaw rate by simultaneously decoupling the lateral aerodynamic force at the tail from the yaw rate. Because the DP is close to the vertical tail for all flight and weight conditions, the lateral acceleration at the tail is approximately decoupled from the yaw rate. Consequently, the main contributions to the shear force at the vertical tail and thereby the shear force are robustly approximately decoupled from the yaw rate.

The decoupled first-order dynamics of the lateral acceleration at the DP and the lateral aerodynamic force at the tail have the additional advantage that any maneuver that the pilot performs in an EO will not excite any complex dynamics, but only moderate transients in loads will occur.

The controller is characterized by a pole-zero cancellation of the Dutch roll mode in the transfer function from the EO moment to the lateral force at the DP. Because the controller depends on varying parameters, the question arises whether a constant controller has approximately the same performance. This can be achieved by an approximate pole-zero cancellation during the robust synergetic controller design. The robust synergetic controller also has to tackle the remaining disturbance term in Eq. (A12).

Acknowledgment

The work of M. Kordt was supported in part by the Airport Frankfurt Main Foundation (Flughafin Frankfurt Main Stiftung).

References

[1]Hopkins, H., "Delivered with Feeling," *Flight International*, Vol. 20, 1991, pp. 31–38.

[2]Joint Aviation Authority, *Joint Aviation Requirements JAR-25 Large Aeroplanes*, Change 14, Printing and Publication Services, Greville House, Cheltenham, U.K., May 1994, p. 1–C–8.

[3]Lomax, T. D., *Structural Loads Analysis for Commercial Transport Aircraft: Theory and Practice*, AIAA Education Series, AIAA, Reston, VA, 1995, pp. 42–45, 143–160.

[4]Favre, C., "Modern Flight Control System—A Pilot Partner Towards Better Safety," *Proceedings of the 2nd International Symposium on Aerospace, Science, and Technology, ISASTI 96*, Science and Technology Ag. of Indonesia, Djakarta, Indonesia, 1996, pp. 472–481.

[5]McLean, D., "An Automatic Engine–Out Recovery System," *Proceedings of the International Aviation Safety Conference, IASC 97*, edited by H. Soekkha, Amsterdam, 1997, pp. 763–776.

[6]Bennani, S., Magni, C. F., and Terlouw, J. C., *Robust Flight Control*, Springer, London, 1997, pp. 149–397.

[7]Joos, H.-D., "Multi-Objective Parameter Synthesis (MOPS)," RCAM (Research Cargo Aircraft Model) Design Challenge Presentation Document, Garteur FM(AG08), National Aerospace Lab., The Netherlands, 1996.

[8]Bennani, S., Magni, J. F., and Terlouw, J. C., *Robust Flight Control*, Springer, London, 1997, pp. 13–21.

[9]Kubica, F., Livet, T., Le Tron, X., and Bucharels, A., "Parameter Robust Flight Control System for a Flexible Aircraft," *Proceedings of the IFAC Conference on Automatic Control in Aerospace*, Elsevier Science Ltd., Oxford, U.K., 1994, pp. 41–45.

[10]Ackermann, J., *Robust Control*, Springer-Verlag, Berlin, 1993, pp. 307–353.

[11]Franklin, G., and Ackermann, J., "Robust Flight Control: A Design Example," *Journal of Guidance and Control*, Vol. 4, 1981, pp. 597–605.

[12]Lambregts, A. A., "Integrated System Design for Flight and Propulsion Control Using Total Energy Principles," AIAA Paper 83-2561, Oct. 1983.

[13]Etkin, B., *Dynamics of Atmospheric Flight*, Wiley, New York, 1972, pp. 101–114, 129–154, 219–256, 280–295.

[14]McLean, D., *Automatic Flight Control Systems*, Prentice Hall International, London, 1990, pp. 16–101, 270–316.

[15]Kaminer, I., Khargonekar, P. P., and Robel, G., "Design of Localizer Capture and Track Modes for a Lateral Autopilot Using H^{∞}-Synthesis," *Proceedings of the American Control Conference*, Vol. 1, American Automatic Control Council, Tampu, FL, 1989, pp. 485–494.